J. Fluid Mech. (1972), *vol.* 53, *part* 4, *pp.* 715–735
Printed in Great Britain

Thermocapillary flow near a hemispherical bubble on a heated wall

By Y. S. KAO† AND D. B. R. KENNING
Department of Engineering Science, Oxford University

(Received 8 December 1971)

The flow driven by variations in surface tension round a hemispherical gas or vapour bubble on a heated wall has been investigated numerically for steady-state conditions over a wide range of values of dimensionless parameters, and experimentally for one set of conditions. Although six parameters are needed to specify the flow conditions, the magnitude of the liquid flow normal to the heated wall is determined primarily by the Marangoni number, Prandtl number and the Biot number based on the effective heat-transfer coefficient at the liquid–gas interface. The interior temperature of the bubble depends in addition on the thermal conductivity ratio of the liquid and the wall material. The flow is very sensitive to the presence of surface-active contaminants. For water, calculations and experimental observations both indicate that contamination which lowers the static surface tension by only 0·1 % may suppress the thermocapillary motion.

1. Introduction

When a small gas bubble rests on a heated wall the difference in surface temperature between its base and tip causes a surface tension gradient which induces a jet-like flow of liquid away from the wall along the bubble axis, see figure 1. Although the net surface tension force on an element of the interface is opposed by viscous shear stresses in both bulk phases, the shear stress in the liquid is generally much larger than that in the gas, which is therefore neglected. The dimensionless parameters defining the flow are then the liquid Prandtl number Pr and the Marangoni number

$$Ma = -\frac{a^2 q}{k\alpha\mu}\frac{d\gamma}{dT}, \tag{1}$$

where a is the bubble radius, q the wall heat flux measured at a position not influenced by the presence of the bubble, and the liquid has thermal conductivity k, thermal diffusivity α, viscosity μ and surface tension γ. (The temperature coefficient of surface tension $d\gamma/dT$ is negative for pure liquids.) The Marangoni number can be regarded as the product of Prandtl number and a Reynolds number with characteristic velocity V defined by relating the viscous shear stress to the surface tension gradient:

$$\frac{\mu V}{a} = -\frac{q}{k}\frac{d\gamma}{dT}. \tag{2}$$

† Present address: Department of Mechanical Engineering, University of British Columbia.

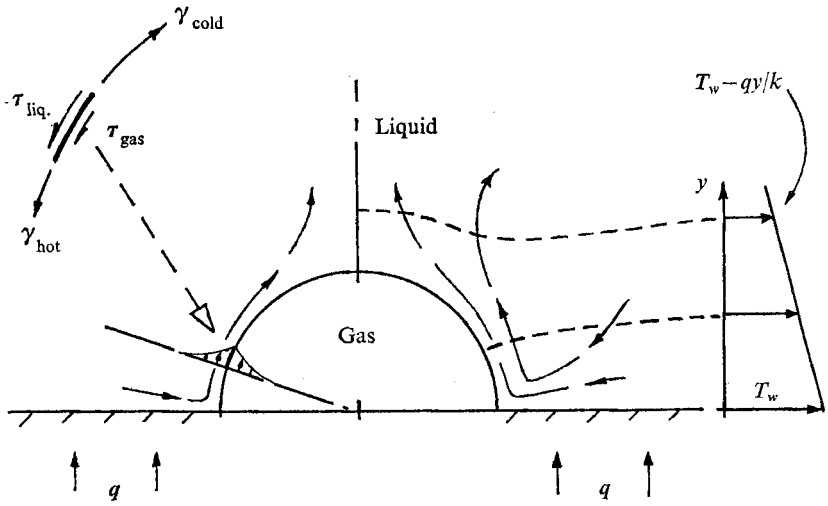

FIGURE 1. Mechanism of thermocapillary motion.

For vapour bubbles, evaporation and condensation at different parts of the surface reduce the temperature differences driving the flow. Following the method of Gaddis & Hall (1968), this situation is handled analytically by using an effective interfacial heat-transfer coefficient h_i between the liquid at the interface and the interior of the vapour phase, derived from kinetic theory by Schrage (1953) as approximately

$$h_i = \frac{2\sigma}{2-\sigma} \frac{h_{fg}}{(2\pi RT)^{\frac{1}{2}}} \left[\left(\frac{dp}{dT} \right) - \frac{p}{2T} \right], \tag{3}$$

where σ is the accommodation coefficient, h_{fg} the latent heat, R the gas constant for the vapour and T and p the saturation temperature and pressure respectively. (Gaddis & Hall neglected the mean vapour velocity relative to the interface and obtained a similar expression for h_i with $2\sigma/(2-\sigma)$ replaced by σ.) The widely differing values of the accommodation coefficient σ which have been reported for water cause some difficulty in calculating h_i from (3). The value of σ has been the subject of recent investigation in connexion with the condensation of liquid metals and indications are that it is close to unity for clean interfaces (Wilcox & Rohsenow 1969), but that its apparent value is much reduced by the accumulation of permanent gases at the interface and by surface contamination. If water behaves in a similar manner, a pure steam bubble at atmospheric pressure would have a very high interfacial heat-transfer coefficient of about 15 MW/m^2 °K ($2{\cdot}8 \times 10^6$ B.Th.U./ft^2 h °F) while a gas bubble would have a very low coefficient, leading to a nearly adiabatic boundary condition at its surface. Two dimensionless groups are associated with the heat transfer at the interface: the Biot number

$$Bi = ah_i/k \tag{4}$$

gives the ratio of the thermal conductances through the bubble and through the surrounding liquid, while the second group ϵ, containing the liquid specific heat c, and defined by

$$\epsilon = a^2 c h_i q / h_{fg} k^2, \tag{5}$$

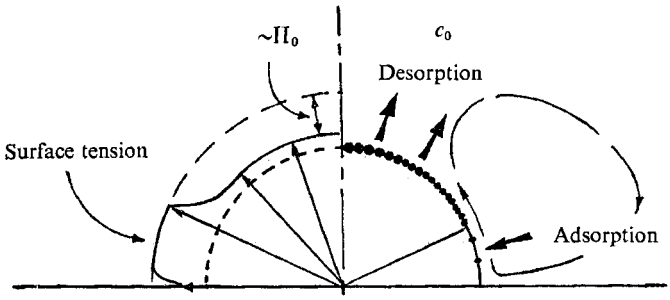

FIGURE 2. Suppression of flow by a surface film.

is a measure of convection due to the liquid motion induced by evaporation and condensation at the interface. Most of the surface tension difference which is the primary cause of fluid motion develops close to the liquid–vapour–solid interface and is affected by the ratio of the liquid and solid thermal conductivities, $K = k_l/k_s$. For relatively large bubbles natural convection effects become significant, depending on the Rayleigh number

$$Ra = a^4 gq\beta\rho/k\alpha\mu, \tag{6}$$

where g is the gravitational acceleration and β the thermal expansion coefficient of the liquid. The equations and boundary conditions containing these groups and the methods employed for their solution are summarized by one of us (Y.S.K.) in the appendix and are discussed in detail by Kao (1970).

McGrew, Bamford & Rehm (1966) and Brown (1967) have suggested that thermocapillary flows might be an important mechanism of heat transfer in boiling; Larkin (1970) emphasized their possible significance in low gravity situations while Gaddis (1968) discussed their indirect effect on heat transfer by influencing the conditions for bubble nucleation. Larkin obtained time-dependent numerical solutions for the flow at $0 \leqslant Ma \leqslant 10^5$, $Pr = 1, 5$ near a gas bubble ($Bi = 0$) on a wall with a constant-heat-flux boundary condition for an initially isothermal system. He found that the flow built up quickly then gradually declined with time but he was unable to continue the solution until a steady-state was reached because of the enormous amount of computer time required. Gaddis obtained series and finite-difference numerical solutions for the steady-state flow round a bubble on an isothermal wall at $0 \leqslant Ma \leqslant 125$, $0 \leqslant Bi \leqslant 100$, the range of interest for bubble nuclei in boiling water. The present investigation extends Gaddis's steady-state solutions to $0 \leqslant Ma \leqslant 2{\cdot}5 \times 10^5$, $0 \leqslant Bi \leqslant 5000$ and examines the effect of local temperature variations in the solid wall. The calculated flow patterns compare satisfactorily with flow visualization experiments on a gas bubble at Marangoni numbers of about 10^4. Limited computer time precluded the numerical investigation of transient conditions.

Liquids are rarely entirely free of soluble surface-active contaminants (surfactants) which tend to suppress the flow caused by surface temperature gradients. The contaminants adsorb on the bubble, forming a surface film which is carried by the flow towards the tip of the bubble, figure 2. Since the film can escape only

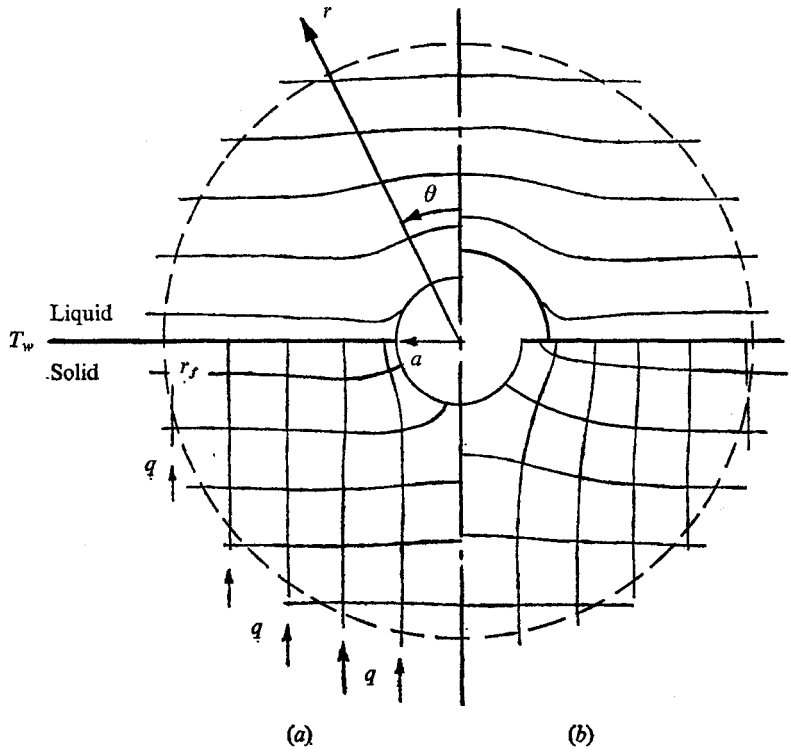

FIGURE 3. Theoretical model.

by a relatively slow process of desorption and diffusion it produces a boundary condition of near-zero velocity over the top part of the bubble. Any liquid flow generated near the bubble compresses the film, causing variations in the concentration of the surfactant with accompanying surface tension gradients which override the effects of temperature gradients and oppose the flow. Although some flow is necessary to compress the film, it may be confined to such a small region as to be undetectable when contamination exceeds a certain level. The thermocapillary flow has been calculated for bubbles with stagnant caps of varying extent to obtain order-of-magnitude estimates of the effects of contamination. Again the estimates are in reasonable agreement with experiments on gas bubbles. Because of the non-uniform distribution of the contaminant at the interface analyses regarding such systems as pure fluids, using temperature coefficients of surface tension for the surfactant solutions measured under static conditions, are invalid.

2. Method of analysis

The energy and Navier–Stokes equations for the liquid and the conduction equation for the solid wall were written in finite-difference form and solved numerically (see appendix) for a bubble positioned over a hemispherical cavity in a thick wall heated by a uniform flux on its rear surface, see figure 3 (*a*). This

Radius (cm)	Heat flux (W/cm^2)	Ma	Bi	ϵ	Ra
10^{-2}	300	$1{\cdot}8\times10^{5}$	$2{\cdot}3\times10^{3}$	$1{\cdot}9\times10^{3}$	58
10^{-2}	30	$1{\cdot}8\times10^{4}$	$2{\cdot}3\times10^{3}$	$1{\cdot}9\times10^{2}$	5·8
10^{-3}	300	$1{\cdot}8\times10^{3}$	$2{\cdot}3\times10^{2}$	19	$5{\cdot}8\times10^{-3}$
10^{-3}	30	$1{\cdot}8\times10^{2}$	$2{\cdot}3\times10^{2}$	1·9	$5{\cdot}8\times10^{-4}$
10^{-4}	300	18	23	$1{\cdot}9\times10^{-1}$	$5{\cdot}8\times10^{-7}$
10^{-4}	30	1·8	23	$1{\cdot}9\times10^{-2}$	$5{\cdot}8\times10^{-8}$

TABLE 1. Values of non-dimensional parameters for vapour bubbles in water at 373 °K

geometry is appropriate for bubble nuclei in boiling but it is only an approximation for larger bubbles resting on a wall, see figure 3 (*b*). Distances were made non-dimensional with respect to the bubble radius:

$$r' = r/a, \quad y' = y/a, \tag{7}$$

and temperatures with respect to the temperature difference between the wall and the surface $y' = 1$ in the liquid far from the bubble:

$$T'(r', \theta) = (T_w - T(r, \theta))\, k/aq. \tag{8}$$

Trial solutions showed the importance of using a fine grid near the base and axis of the bubble so a non-uniform spacing was adopted: angular steps $\Delta\theta_1 = 1{\cdot}5°$ were used for $0 \leqslant \theta \leqslant 12°$, $72° \leqslant \theta \leqslant 105°$ and $\Delta\theta_2 = 3{\cdot}0°$ for $12° \leqslant \theta \leqslant 72°$, $105° \leqslant \theta \leqslant 180°$. A new radial co-ordinate z was defined by

$$r' = e^{z} \tag{9}$$

and uniform steps $\Delta z = 0{\cdot}054$ were used. The resulting grid near the liquid–vapour–solid interface was much smaller than that used by Larkin (1970) and Gaddis (1968) and gave an error of less than 4% when tested against Gaddis's series solution for bubble temperature at $Ma = 0, Bi = 100$, whereas his numerical solution was in error by 20%. The required boundary conditions distant from the bubble of negligible liquid velocity (zero stream function ψ) and uniform heat flux were applied at finite radial distances from the bubble centre of 8·7 radii for $Ma \leqslant 500$ and 13·3 radii for $Ma > 500$, it being confirmed by trial that this choice had negligible effect on the computed values of maximum stream function and bubble interior temperature. Since the number of dimensionless parameters defining the flow was embarrassingly large it was not feasible to examine all possible combinations of their values. Attention was generally restricted to the ranges of values appropriate to vapour bubbles in water at 373 °K, table 1. The convergence of the numerical solution provided a further constraint when conditions generated strong thermocapillary flows: for $Bi = 0$ computation time became excessive (> 2 hours on the I.C.L. KDF 9 computer) for $Ma > 500$, but for $Bi = 1000$ computation was possible up to $Ma = 2{\cdot}5\times10^{5}$.

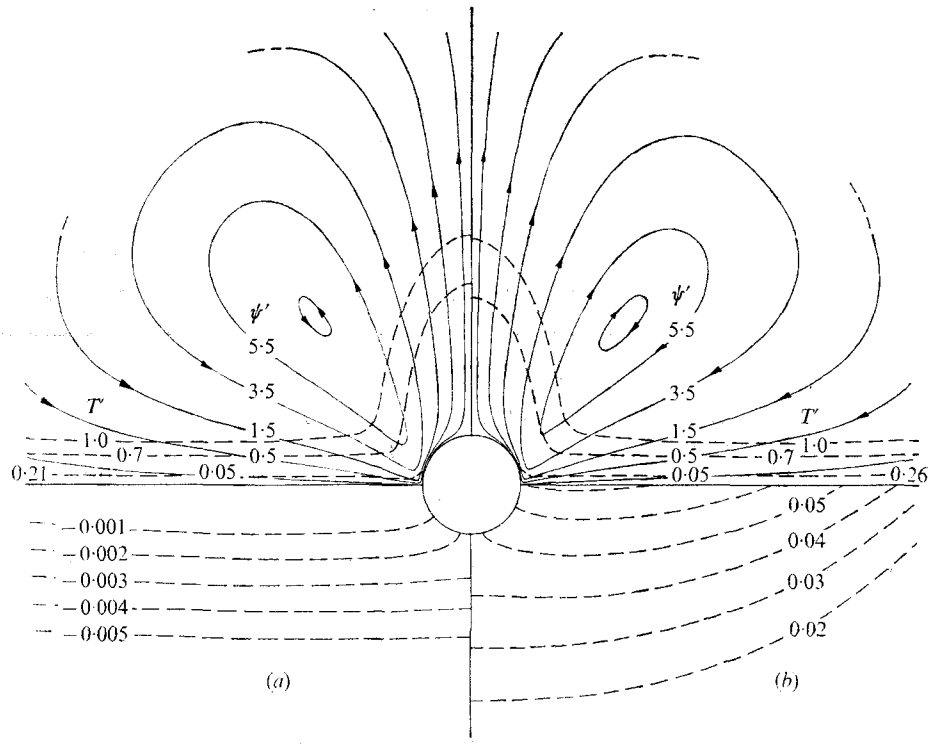

FIGURE 4 (*a*, *b*). For legend see facing page.

3. Discussion of numerical results

For the smaller bubbles in boiling, buoyancy effects on the flow are negligible ($Ra \ll 1$). Typical streamlines and isotherms under these conditions are shown in figure 4. Liquid flows along the wall towards the base of the bubble, where it is sharply accelerated by surface tension gradients in the region $80° \leqslant \theta \leqslant 90°$, forming a jet normal to the wall. The jet diffuses, creating a ring vortex round the bubble axis. The strength of the thermocapillary flow is measured by the maximum value of the non-dimensional stream function ψ'_m at the centre-line of the vortex, ψ'_m being defined by

$$\psi'_m = \psi_m / a\alpha, \tag{10}$$

where ψ is the (dimensional) stream function representing the volumetric flow of liquid. For steady-state conditions there is no net heat transfer to the bubble, evaporation at its base being equal to the condensation at its tip. The isotherm separating these regions corresponds to the temperature of the vapour in the interior of the bubble T'_v and far from the bubble reaches a distance from the wall $y'_v = T'_v$. (Note that an increase in T'_v corresponds to a reduction in bubble temperature relative to the wall temperature.) Isotherms in the liquid close to the wall suffer little distortion except very close to the bubble base so it is only in this limited region that there is a significant increase in the wall heat flux, see figure 5. Evaporation and condensation at the bubble surface cause some motion of the liquid but over the range of parameter values

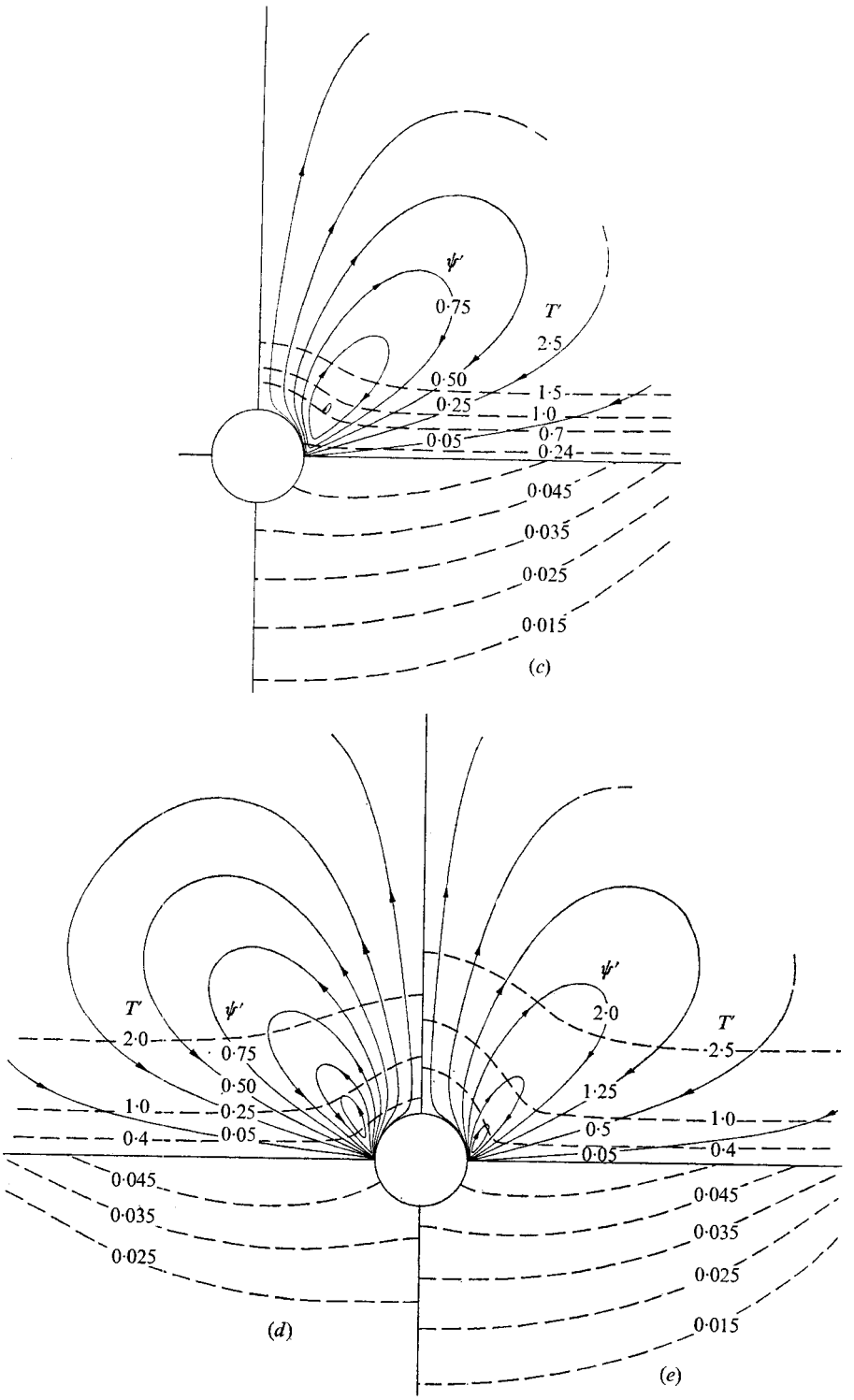

FIGURE 4. Calculated streamlines and isotherms for a pure liquid, buoyancy effects negligible, $Ra = 0$, $Pr = 1{\cdot}75$.

	(a)	(b)	(c)	(d)	(e)
Ma	2 050	2 050	2 050	25 000	250 000
Bi	11·3	11·3	113	1 000	1 000
ϵ	0	0	0	136	1 362
K	0·00177	0·0152	0·0152	0·0152	0·0152

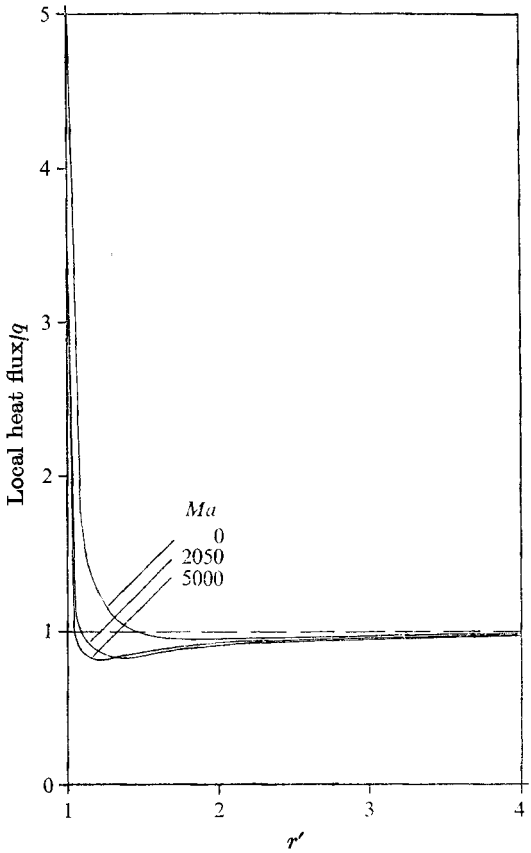

FIGURE 5. Local variations in wall heat flux. $Bi = 113$, $Ra = 0$, $Pr = 1{\cdot}75$, $\epsilon = 0$, $K = 0{\cdot}0152$.

examined this effect is small compared with the thermocapillary flow and most calculations were performed with $\epsilon = 0$. The conductivity ratio K has a significant effect on the temperature distribution but not on the flow pattern or strength. Most calculations were performed with $K = 0{\cdot}015$ (water on steel), with a few calculations at $K = 0{\cdot}0018$ (water on copper) and $K = 0$. For calculation of T'_v the limiting value $K = 0$ (isothermal wall surface) can be assumed only for $Ma \ll 500$; otherwise increasing K reduces the bubble temperature relative to the wall temperature (increased $y'_v = T'_v$) and slightly reduces the flow rate.

Variations in the Marangoni and Biot numbers do not greatly alter the flow pattern but do cause large changes in the magnitude of the velocities. For a Prandtl number of 1·75 and $0 \leqslant K \leqslant 0{\cdot}015$ the non-dimensional flow rate is given approximately by the empirical expression

$$\psi'_m = 0{\cdot}17(Ma/Bi)^{\frac{2}{3}} \tag{11}$$

for $5 \leqslant Ma/Bi \leqslant 200$, $61 \leqslant Ma \leqslant 5 \times 10^4$ (figure 6), but the one calculation at a still higher Ma of 250 000 gave a flow 50 % below this correlation. The changes in bubble equilibrium temperature do not follow such a straightforward pattern, ranging from increases in T'_v with increasing Biot number at low Marangoni

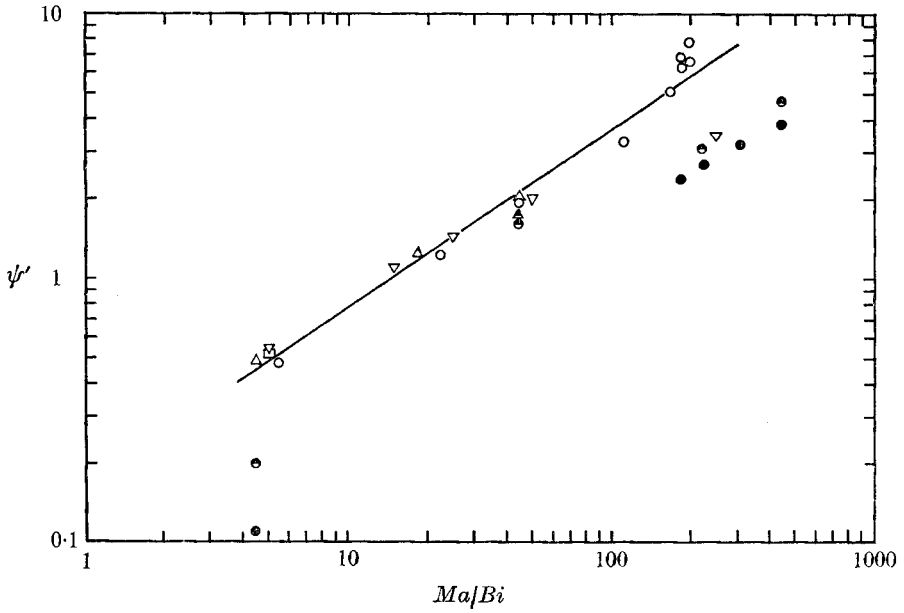

FIGURE 6. Correlation of flow rate calculations. ○, $Bi = 11{\cdot}3$; △, $Bi = 113$; ▽, $Bi = 1000$; □, $Bi = 5000$; ◓, ▲, $\theta_s = 57°$; ●, $\theta_s = 72°$.

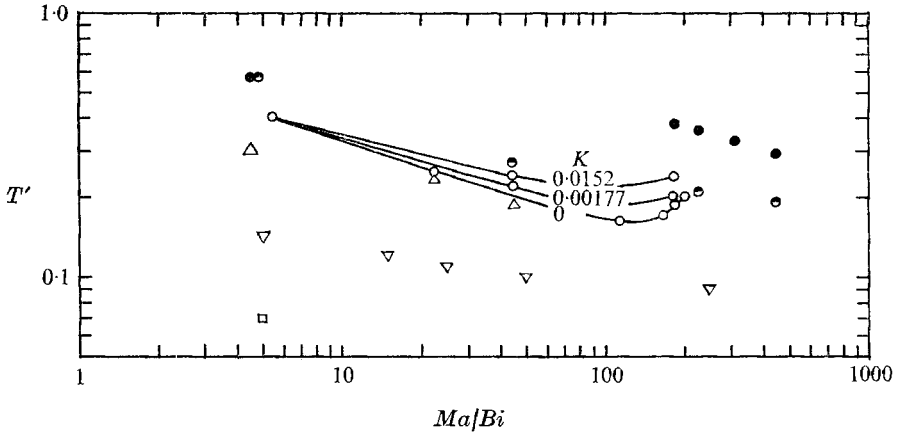

FIGURE 7. Variations in bubble equilibrium temperature ($K = 0{\cdot}0152$ except where indicated). Notation as in figure 6.

number to decreases at higher Bi and Ma, see figure 7. The values of ψ'_m and T'_v for all cases investigated are summarized in table 2. The effects of changing the Prandtl number were not examined in any detail. With the choice of non-dimensional variables used in this work, the Prandtl number appears only as a divisor of the inertia term in the equation of motion of the liquid so this term is significant only at low Pr or at large flow rates. Calculations at $Pr = 15{\cdot}6$ and $Pr = \infty$ (no inertia term) gave values of ψ'_m within 5% of the values at $Pr = 1{\cdot}75$ for $Ma/Bi \leqslant 50$ but gave values decreased by 40% at $Ma/Bi = 180$. Larkin (1970) found a similar decrease in local velocities in going from $Pr = 1$ to $Pr = 5$ at

Ma	Bi	Pr	κ	ϵ	Ra	θ_s	ψ'_m	T'_v
50	0	1·75	0·0152	0	0	0	1·10	—
500	0	1·75	0·0152	0	0	0	15·2	—
500	0	1·75	0·00177	0	0	0	15·9	—
61	11·3	1·75	0	0	0	0	0·48	0·40
250	11·3	1·75	0	0	0	0	1·22	0·25
500	11·3	1·75	0	0	0	0	1·95	0·22
1 250	11·3	1·75	0	0	0	0	3·3	0·16
1 875	11·3	1·75	0	0	0	0	5·1	0·17
2 050	11·3	1·75	0	0	0	0	6·9	0·19
2 250	11·3	1·75	0	0	0	0	7·9	0·20
500	11·3	1·75	0·0152	0	0	0	1·95	0·24
500	11·3	1·75	0·00177	0	0	0	1·95	0·22
2 050	11·3	1·75	0·0152	0	0	0	6·3	0·24
2 050	11·3	1·75	0·00177	0	0	0	6·7	0·20
500	113	1·75	0·0152	0	0	0	0·49	0·30
500	113	1·75	0·00177	0	0	0	0·50	0·27
2 050	113	1·75	0·0152	0	0	0	1·26	0·24
5 000	113	1·75	0·0152	0	0	0	2·05	0·19
2 050	11·3	15·4	0·0034	0	0	0	6·35	0·24
61	11·3	∞	0	0	0	0	0·48	0·40
125	10·0	∞	0·0152	0·68	0	0	0·85	0·40
2 050	11·3	∞	0·0152	0	0	0	3·6	0·20
5 000	113	∞	0·0152	0	0	0	2·0	0·19
2 050	113	1·75	0·0152	11·2	0	0	1·25	0·23
5 000	113	1·75	0·0152	27·2	0	0	2·0	0·19
5 000	1 000	1·75	0·0152	27·2	0	0	0·55	0·14
15 000	1 000	1·75	0·0152	81·8	0	0	1·12	0·12
25 000	1 000	1·75	0·0152	136	0	0	1·46	0·11
25 000	5 000	1·75	0·0152	136	0	0	0·54	0·07
50 000	1 000	1·75	0·0152	272	0	0	2·0	0·10
250 000	1 000	1·75	0·0152	1362	0	0	3·5	0·09
50	11·3	1·75	0·0152	0	0	72	0·11	0·57
2 050	11·3	1·75	0·0152	0	0	72	2·4	0·38
2 500	11·3	1·75	0·0152	0	0	72	2·7	0·36
3 500	11·3	1·75	0·0152	0	0	72	3·2	0·33
5 000	11·3	1·75	0·0152	0	0	72	3·8	0·29
50	11·3	1·75	0·0152	0	0	57	0·20	0·56
500	11·3	1·75	0·0152	0	0	57	1·6	0·27
2 500	11·3	1·75	0·0152	0	0	57	3·1	0·21
5 000	11·3	1·75	0·0152	0	0	57	4·7	0·19
5 000	113	1·75	0·0152	0	0	57	1·8	0·23
50	11·3	1·75	0·0152	0	0	42	0·31	0·50
2 050	11·3	1·75	0·0152	0	0	42	3·6	0·21
2 050	11·3	1·75	0·0152	0	8·0	0	4·8	0·27
2 500	11·3	1·75	0·0152	0	9·8	0	5·9	0·28
2 500	11·3	1·75	0·0152	0	9·8	57	3·7	0·26
5 000	11·3	1·75	0·0152	0	39·0	57	6·7	0·27

TABLE 2. Summary of numerical results

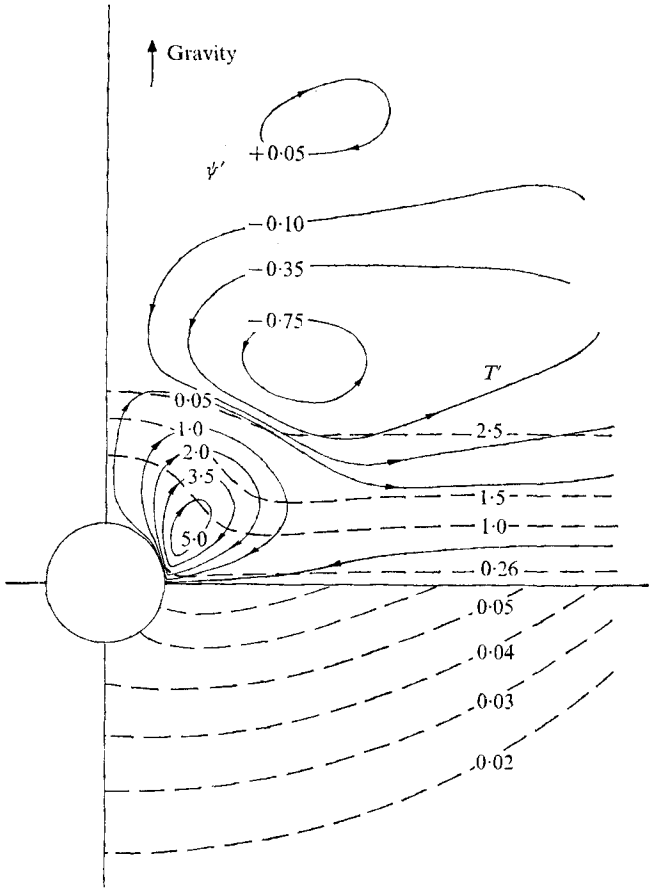

FIGURE 8. Effect of buoyancy, pure liquid. (Orientation inverted for comparison with figure 4.) $Ma = 2050$, $Bi = 11{\cdot}3$, $Ra = 8{\cdot}0$, $Pr = 1{\cdot}75$, $\epsilon = 0$, $K = 0{\cdot}0152$.

$Ma = 2000$, $Bi = 0$. Equation (11) cannot be used for the limiting case $Bi = 0$; the two calculations at $Pr = 1{\cdot}75$ for this condition suggest the relationship

$$\psi'_m = 0{\cdot}013 Ma^{1{\cdot}14}. \tag{12}$$

It was desired to compare the calculated flows with experimental observations on gas bubbles below a heated plate, described in §5. This orientation was chosen to give a stable liquid layer in the absence of disturbance by the bubble. Observations could be made conveniently only on relatively large bubbles of radius > 1 mm. For this bubble size buoyancy terms in the equation of motion are no longer negligible so calculations were performed at Rayleigh numbers Ra (defined by (6)) up to 39. With increasing Ra the penetration distance of the jet leaving the bubble is reduced; the centre of the primary vortex moves in towards the bubble and weaker secondary vortices appear in the outer region, see figure 8. Although the overall flow pattern is changed, the flow associated with the primary vortex is not greatly affected. Variations in the temperature field are confined to a region closer to the bubble. No calculations were made for conditions under which buoyancy effects assist the thermocapillary flow.

4. Surface contamination

Under conditions of static equilibrium, with no fluid motion whatsoever, the surface concentration Γ molecules per unit area of a soluble surfactant is related to its bulk concentration c_0 in the liquid by the Gibbs adsorption equation

$$\Gamma = \frac{c_0}{2\kappa T}\left(\frac{\partial \Pi_0}{\partial c_0}\right)_T, \tag{13}$$

where κ is the Boltzmann constant and Π_0 is the 'surface pressure', the reduction in surface tension γ. Π_0 is related to Γ by a surface equation of state which for dilute solutions approaches a form equivalent to the ideal gas equation:

$$\Pi_0/\Gamma = \kappa T, \tag{14}$$

with Π_0, Γ and c_0 linearly related. The gradients of surface tension caused by the non-uniform distribution of surfactant at the surface of a non-equilibrium, flowing system can be analysed on the basis of the 'local-equilibrium' hypothesis that the above relationships still apply for an element of the surface and the liquid immediately adjacent to it, although there may be concentration gradients in the bulk phase and a net rate of transfer of surfactant between substrate and surface, i.e. it is assumed that the local rates of adsorption and desorption are controlled entirely by diffusion and convection in the bulk liquid. Even for this linearized model the analysis is formidable, requiring simultaneous solution of the energy, Navier–Stokes and mass-transfer equations for the liquid with boundary conditions generated by the equations of motion and continuity of the surface film. However, further simplifications are possible. In experiments on isothermal flows containing surfactants it is generally found that the surface can be divided into an upstream region in which gradients of surface concentration are negligible (zero surface shear stress) followed by a region of rapid transition to a nearly stagnant downstream region (zero surface velocity). A similar pattern is assumed for the present flow, with the bubble surface covered by a stagnant cap over the region $0 \leqslant \theta_s \leqslant 57°$ or $72°$ but with the temperature and surface tension gradients driving the flow in the wall region being uninfluenced by the presence of surfactant. In the stagnant zone it is known *a posteriori* that surface temperature gradients are an order of magnitude smaller than in the wall region so the interaction of temperature and concentration gradients is not considered. With these boundary conditions the flow can be calculated numerically as before, without the need for simultaneous solutions of the surfactant mass-transfer equations. Since the shear stress in the stagnant part of the surface is equal to the gradient of surface pressure, the variations in surface pressure $\Delta\Pi'$ over this region can be calculated, see figure 9, where surface pressure has been made non-dimensional by the relationship

$$\Pi' = (a/\alpha\mu)\,\Pi. \tag{15}$$

This distribution of surface pressure, and hence of bulk concentration in the adjacent liquid, provides the boundary conditions for the mass transfer of surfactant. The concentration required to maintain the chosen extent of the stagnant cap can then be determined by the method used by Kenning (1968) for

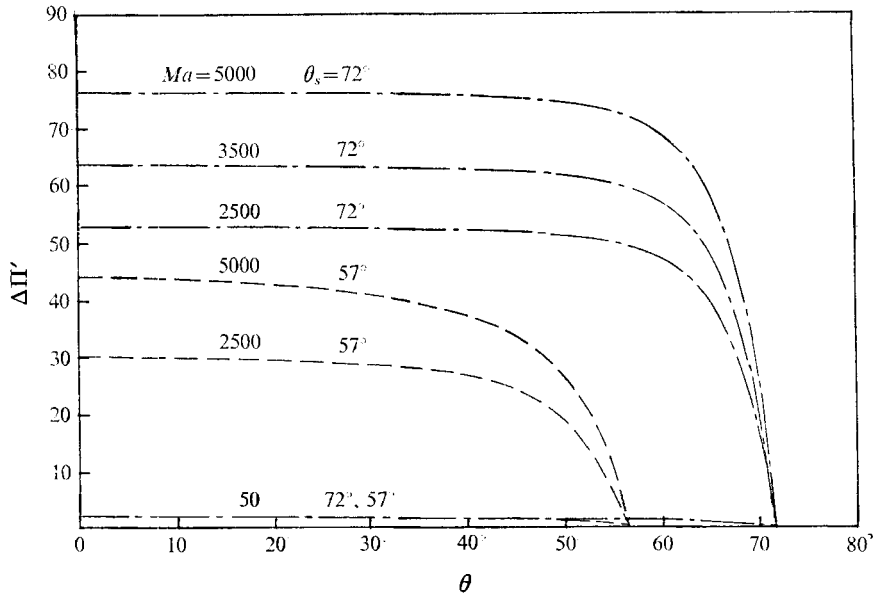

FIGURE 9. Shear stress variation over stagnant cap.

surface film formation in open channel flow. Even this simplified analysis may be of little practical use since values are required for the diffusion coefficient, molecular weight and ratio of surface to bulk concentration of the surface-active contamination and these are generally unknown. The only experimentally convenient measure of the degree of contamination is the surface pressure Π_0 (surface tension lowering) of a sample of the liquid, measured under conditions of static equilibrium. Fortunately figure 9 can be used to obtain an order-of-magnitude estimate of the value of Π_0 needed to produce a stagnant cap, without further information on the properties of the surfactant. The surface pressure differences in the stagnant zone develop close to its leading edge so the surface pressure and the corresponding bulk concentration in the film substrate are nearly constant over $0 \leqslant \theta \leqslant \theta_s$. Because of this large area for mass transfer away from the surface the substrate concentration should not differ greatly from the bulk concentration in the interior of the liquid, which corresponds to a surface pressure of Π_0. For $\theta > \theta_s$, the surface pressure should be very much less than the equilibrium value: surface elements are greatly expanded as they are accelerated away from the wall, reducing the surface concentration of surfactant and leaving little time for replenishment by diffusion from the bulk phase. Thus the total surface pressure difference across the stagnant cap should be nearly equal to the static lowering of surface tension Π_0, irrespective of the precise properties of the contaminant. (This argument is peculiar to this flow configuration; in channel flow, for example, local values of surface pressure at the downstream end of a surface film can exceed the static value by more than an order of magnitude.) In figure 10 calculated values of $\Pi' = (a/\alpha\mu)\,\Pi_0$, equal to the maximum values of $\Delta\Pi'$ in figure 9, are plotted against Ma/Bi for films extending to $\theta_s = 57°$ and $72°$.

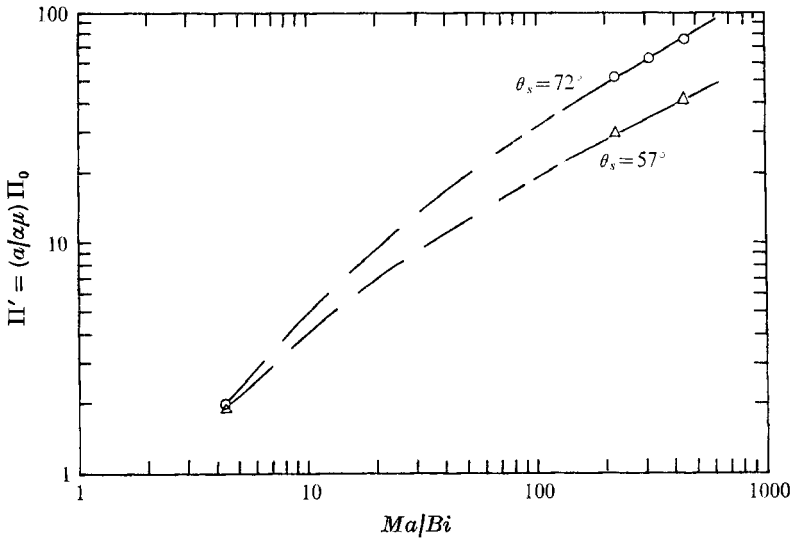

FIGURE 10. Surfactant contamination required to produce stagnant cap.

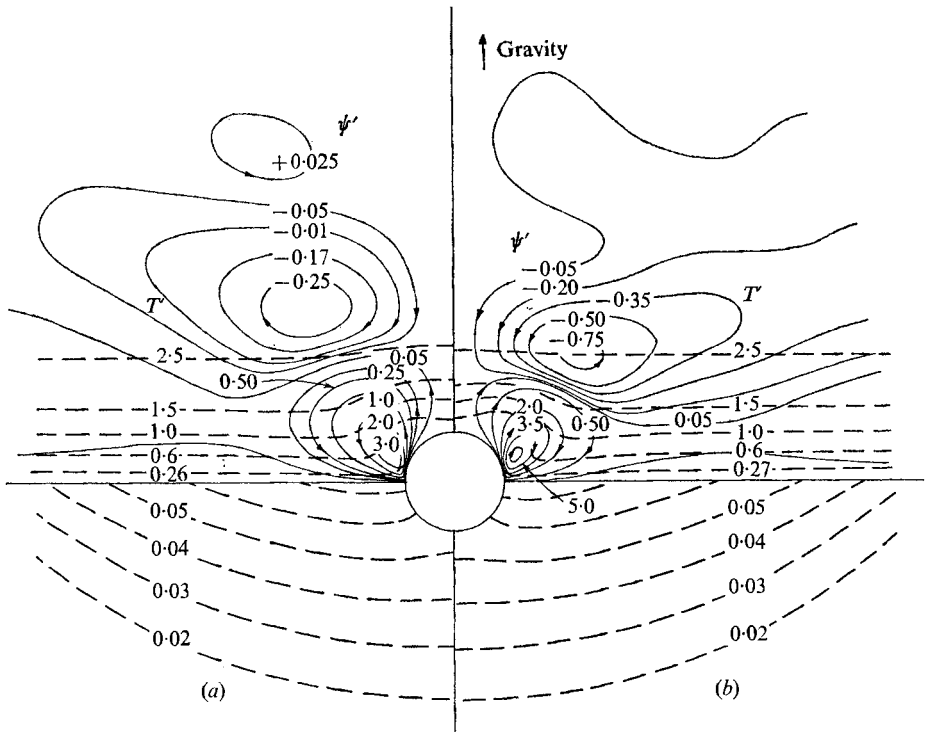

FIGURE 11. Calculated streamlines and isotherms with buoyancy effects and stagnant cap; $\theta_s = 57°, Bi = 11{\cdot}3, Pr = 1{\cdot}75, \epsilon = 0, K = 0{\cdot}0152$. (*a*) $Ma = 2500, Ra = 9{\cdot}8$. (*b*) $Ma = 5000, Ra = 38{\cdot}9$.

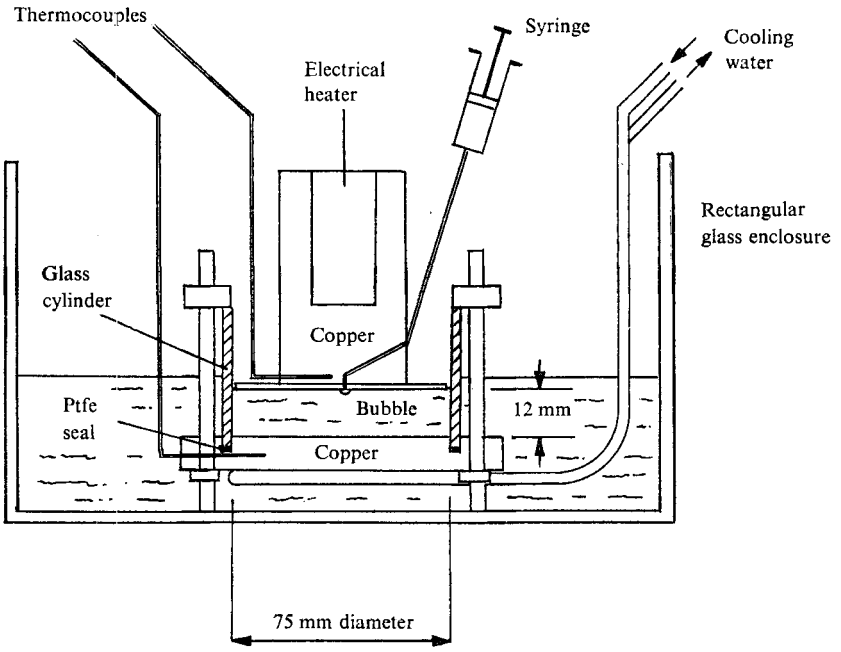

FIGURE 12. Experimental apparatus.

No calculations were performed for the limiting case $Bi = 0$ but appropriate values of Π' can be read from figure 10 at values of Ma/Bi corresponding to the same flow rate ψ'_m, since this should give approximately the same shear stresses on the stagnant film. For a 1 mm radius gas bubble in water at $10^3 \leqslant Ma \leqslant 10^4$ (conditions of the experiments to be described in §5) the calculated range of Π_0 is 3×10^{-2} to 3×10^{-1} dyn/cm, a surface tension lowering of around 0·1 %. The presence of a stagnant film reduces the mass flow of liquid considerably, see figure 6, particularly at low Ma/Bi. With gravitational effects also present, circulation is significant only in a region close to the bubble, having little effect on the temperature distribution elsewhere, see figure 11.

5. Experimental work

The thermocapillary flow near a bubble was investigated with the apparatus shown in figure 12. An air bubble blown with a syringe through a hole in the upper heated plate was used rather than a vapour bubble since it conveniently gave steady-state conditions, although excluding any study of the effect of Biot number. The liquid flow was made visible by suspended 'Eccospheres', hollow glass beads of 25 μm diameter. It was essential to use a flow tracer which did not accumulate at the bubble surface and Eccospheres were satisfactory in this respect in water (but not in methanol). The tracers were illuminated by a thin plane of light traversing the bubble axis and were photographed with a 35 mm camera at 1:1 magnification using an exposure of 1 s at f/4. The light source was a mercury vapour lamp flashing at 100 Hz so velocity measurements could be obtained from the interrupted particle paths.

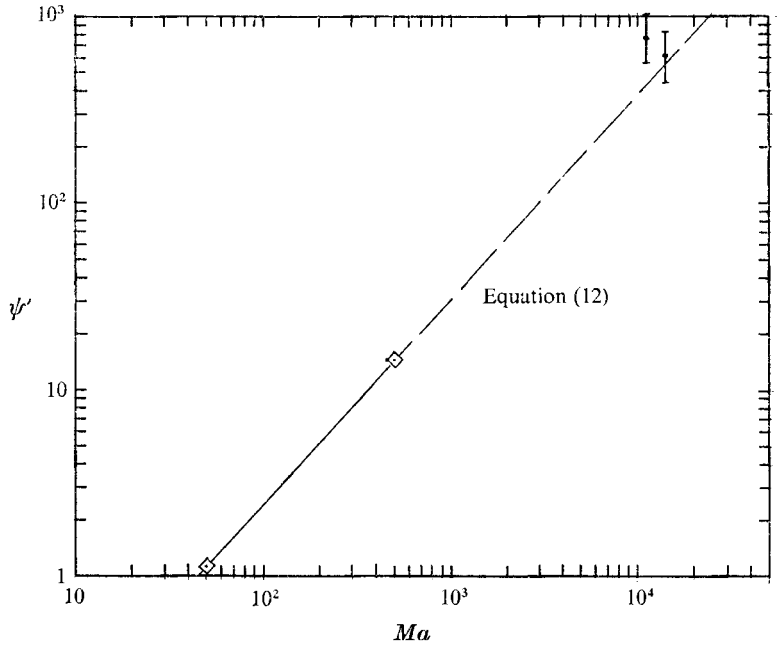

FIGURE 14. Experimental and theoretical flow rates. ⧳, experimental, $Pr \simeq 4{\cdot}5$; ◇, computed, $Pr = 1{\cdot}75$, $Bi = 0$.

It was known from the estimates of the previous section that thermocapillary flows would be observable only if stringent precautions were taken to exclude surfactants. The water was distilled, passed through a 'Bio-deminrolit' ion-exchange column, distilled with alkaline permanganate and finally redistilled. Its surface tension was within 0·2 dyn/cm of the International Critical Tables value for pure water, but could not be measured more accurately. The apparatus was constructed of copper, glass and ptfe, and was cleaned by immersion in warm chromic acid. It was often necessary to repeat the cleaning procedure several times to eliminate contamination: the only reliable test of the cleanliness of the equipment was the subsequent behaviour of the thermocapillary flow itself. This is consistent with the estimates of the previous section that the level of contamination producing significant effects for these experiments corresponds to a surface tension lowering of somewhat less than 0·1 dyn/cm.

A typical steady-state flow pattern is shown in figure 13 (plate 1) and follows the calculated pattern. Values of ψ'_m obtained from the flow traces are shown in figure 14 and lie close to the extrapolation of the calculated values. A direct comparison was not possible: with $Bi = 0$ the numerical calculations were limited by convergence problems to $Ma < 500$ and at such low values of Ma even the very small amount of residual surfactant in the water was sufficient to suppress most of the thermocapillary motion. At rather higher Ma the flow was partially suppressed so a stagnant cap could be observed on the bubble, see figure 15 (plate 1). The presence of a cap covering only a small part of the bubble surface appeared to cause flow instabilities; the edge of the cap fluctuated and the flow

leaving the bubble swung from side to side, figure 16 (plate 2). The irregular motion of small rising bubbles may be due to a similar instability.

Although transient conditions were not calculated they were studied experimentally for two different initial conditions. Following injection of a bubble into an established temperature gradient there was a strong initial thermocapillary flow with streamlines approaching the bubble at greater distances from the wall than in the steady state, see figure 17 (plate 2). The flow then declined somewhat to the steady-state value over a period of about 150 s. Similar behaviour occurred if the gas bubble was formed in an isothermal system and heating then applied to the wall, except that the period for establishment of the flow was rather longer owing to the thermal capacity of the heater. Qualitatively, the behaviour agreed with Larkin's (1970) calculations for liquid hydrogen. However, for water contaminated with surfactant the initial conditions could produce considerable differences in behaviour. For tap water with $\Pi_0 \simeq 1$ dyn/cm injection of a bubble into an existing temperature gradient produced a thermocapillary flow which gradually died out over a period of about 120 s, while no flow at all occurred with an isothermal initial condition. The longer contact time in the second case evidently allowed the formation of a surface film which inhibited all thermocapillary motion. The surfactant properties certainly affect this behaviour, although this aspect of the problem was not investigated: with an inadequately cleaned system (but with $\Pi_0 \ll 1$ dyn/cm) the flow was often suppressed even on bubbles newly injected into an established temperature gradient.

6. Conclusion

At $Pr = 1{\cdot}75$ the liquid flow caused by a hemispherical vapour bubble is given by equation (11), but approaches the values given by equation (12) for low heat-transfer coefficients at the bubble surface, e.g. for gas bubbles. An increase in Prandtl number tends to reduce the flow, but only at relatively high flow rates when inertia terms in the equation of motion are significant. Although the flow rate generated by a bubble near the wall is not greatly affected by an opposing gravitational field the penetration of the hot jet into the surrounding liquid is reduced for $Ra > 1$, approximately. Steady-state thermocapillary flows are easily suppressed by surface-active contaminants, often at concentrations too low to be detected by surface tension measurements. Under transient conditions the flow rate may initially exceed its final value by rather less than 50 %. Surfactant contamination sufficient to suppress the steady-state flow may still permit some thermocapillary flow when a bubble is first injected into an established temperature gradient, but further investigation of the effects of surfactant properties and concentration is required.

This work was supported by Babcock & Wilcox (Operations) Ltd.

Appendix. Summary of equations and method of solution

Following the method of Jenson (1959), the Navier–Stokes equation for the liquid phase (including a buoyancy term) is rewritten with stream function ψ and vorticity ω as functions of the spherical co-ordinates r and θ. These variables and the radial velocity u, tangential velocity v and temperature T are given non-dimensional values (denoted by a prime) as follows:

$$\left.\begin{aligned} \psi' &= \psi/a\alpha, & \omega' &= a^2\omega/\alpha, \\ u' &= au/\alpha, & v' &= av/\alpha, \\ T' &= (T_w - T)\,k/aq, & r' &= r/a. \end{aligned}\right\} \tag{A 1}$$

The equations then become

$$Pr^{-1} r' \sin^2\theta \left[u' r' \frac{\partial}{\partial r'}\left(\frac{\omega'}{r'\sin\theta}\right) + v' \frac{\partial}{\partial\theta}\left(\frac{\omega'}{r'\sin\theta}\right)\right]$$
$$= E^2 (r'\omega' \sin\theta) - Ra\, r' \sin\theta \left[\sin\theta \frac{\partial T_l'}{\partial r'} + \frac{\cos\theta}{r'} \frac{\partial T_l'}{\partial\theta}\right], \tag{A 2}$$

$$E^2 \psi' = r'\omega' \sin\theta, \tag{A 3}$$

$$u' \frac{\partial T_l'}{\partial r'} + \frac{v'}{r'} \frac{\partial T_l'}{\partial\theta} = \nabla^2 T_l', \quad 0 \leqslant \theta \leqslant \tfrac{1}{2}\pi \quad \text{(liquid)}, \tag{A 4}$$

$$\nabla^2 T_s' = 0, \quad \tfrac{1}{2}\pi \leqslant \theta \leqslant \pi \quad \text{(solid)}, \tag{A 5}$$

where
$$u' = -\frac{1}{r'^2 \sin\theta} \frac{\partial\psi'}{\partial\theta}, \quad v' = \frac{1}{r'\sin\theta} \frac{\partial\psi'}{\partial r'}, \tag{A 6), (A 7}$$

$$E^2 = \frac{\partial^2}{\partial r'^2} + \frac{\sin\theta}{r'^2} \frac{\partial}{\partial\theta}\left(\frac{1}{\sin\theta} \frac{\partial}{\partial\theta}\right), \tag{A 8}$$

$$\nabla^2 = \frac{\partial^2}{\partial r'^2} + \frac{2}{r'} \frac{\partial}{\partial r'} + \frac{1}{r'^2} \frac{\partial^2}{\partial\theta^2} + \frac{1}{r'^2} \cot\theta \frac{\partial}{\partial\theta} \tag{A 9}$$

(variables u' and v' are retained for convenience in the subsequent numerical operations).

The boundary conditions are as follows.

(*a*) At large distances the disturbance due to the presence of the bubble dies away: the liquid is at rest; the temperature gradient in the liquid and wall is uniform. For the purposes of numerical calculation these conditions are applied at a finite reference radius r_f': at $r' = r_f'$

$$\psi' = 0, \quad \omega' = 0 \tag{A 10), (A 11}$$

$$T_l' = r_f' \cos\theta, \quad 0 \leqslant \theta \leqslant \tfrac{1}{2}\pi, \tag{A 12}$$

$$T_s' = K r_f' \cos\theta, \quad \tfrac{1}{2}\pi \leqslant \theta \leqslant \pi. \tag{A 13}$$

(*b*) At the liquid–solid interface the liquid is stationary and temperatures and normal components of heat flux are equal in the liquid and solid. For $\theta = \frac{1}{2}\pi$, $r' \geqslant 1$

$$\psi' = 0, \quad \omega' = \frac{1}{r'^3} \frac{\partial^2\psi'}{\partial\theta^2}, \tag{A 14), (A 15}$$

$$T_s' = T_l', \quad \frac{\partial T_s'}{\partial\theta} = K \frac{\partial T_l'}{\partial\theta}. \tag{A 16), (A 17}$$

(*c*) At the liquid-gas interface the surface tension gradient is equal to the viscous shear stress in the liquid and the radial component of liquid velocity depends on the local rate of heat transfer. The conduction heat flux in the liquid is equal to the evaporation (or condensation) heat flux between the interface and the interior of the bubble at temperature T'_v; the net heat flow into the bubble is zero for the steady state. So for $r' = 1$, $0 \leqslant \theta \leqslant \frac{1}{2}\pi$

$$\omega' = Ma\frac{\partial T'_l}{\partial \theta} + \frac{2}{\sin\theta}\left(\frac{\partial^2 \psi'}{\partial r'^2} - \frac{\partial \psi'}{\partial r'}\right), \tag{A 18}$$

$$\psi' = \epsilon\left[(1-\cos\theta)\,T'_v - \int_{\substack{0\\ r'=1}}^{\theta} T'_l \sin\theta\, d\theta\right], \tag{A 19}$$

$$\partial T'_l/\partial r' = Bi[T'_l - T'_v], \tag{A 20}$$

$$T'_v = \int_{\substack{0\\ r'=1}}^{\frac{1}{2}\pi} T'_l \sin\theta\, d\theta. \tag{A 21}$$

For bubbles with a stagnant cap over the region $0 \leqslant \theta \leqslant \theta$ (A 18) applies only for $\theta > \theta_s$, with

$$v' = 0 \quad \text{for} \quad r' = 1, \quad 0 \leqslant \theta \leqslant \theta_s. \tag{A 22}$$

(*d*) At the solid–gas interface heat transfer is assumed negligible:

$$\partial T'_s/\partial r' = 0 \quad \text{for} \quad r' = 1, \ \tfrac{1}{2}\pi \leqslant \theta \leqslant \pi. \tag{A 23}$$

(*e*) On the axis of symmetry

$$\psi' = \omega' = \partial T'_l/\partial\theta = 0 \quad \text{for} \quad \theta = 0, \tag{A 24}$$

$$\partial T'_s/\partial\theta = 0 \quad \text{for} \quad \theta = \pi. \tag{A 25}$$

Since a grid with mesh size increasing radially is required for the finite-difference equations, a new co-ordinate z is defined by

$$r' = e^z, \tag{A 26}$$

transforming the equations to

$$Pr^{-1} e^{3z}\sin^2\theta\left(u'\frac{\partial F}{\partial z} + v'\frac{\partial F}{\partial\theta}\right) = e^{3z}E^2 G - Ra\, e^{2z}\sin\theta\left[\sin\theta\frac{\partial T'_l}{\partial z} + \cos\theta\frac{\partial T'_l}{\partial\theta}\right], \tag{A 27}$$

$$e^{2z}E^2\psi' = e^{2z}G, \tag{A 28}$$

$$e^z\left[u'\frac{\partial T'_l}{\partial z} + v'\frac{\partial T'_l}{\partial\theta}\right] = \frac{\partial^2 T'_l}{\partial z^2} + \frac{\partial T'_l}{\partial z} + \frac{\partial^2 T'_l}{\partial\theta^2} + \cot\theta\frac{\partial T'_l}{\partial\theta}, \tag{A 29}$$

$$\frac{\partial^2 T'_s}{\partial z^2} + \frac{\partial T'_s}{\partial z} + \frac{\partial^2 T'_s}{\partial\theta^2} + \cot\theta\frac{\partial T'_s}{\partial\theta} = 0, \tag{A 30}$$

where

$$e^{2z}E^2 = \frac{\partial^2}{\partial z^2} - \frac{\partial}{\partial z} + \frac{\partial^2}{\partial\theta^2} - \cot\theta\frac{\partial}{\partial\theta}, \tag{A 31}$$

$$F = \omega'/e^z\sin\theta, \tag{A 32}$$

$$G = \omega' e^z\sin\theta = e^{2z}\sin^2\theta F. \tag{A 33}$$

The boundary conditions become the following.

(*a*) On $z = z_f$, equation (A 10) is still appropriate and

$$F = G = 0, \tag{A 34}$$

$$T'_l = e^{z_f} \cos\theta, \quad 0 \leqslant \theta \leqslant \tfrac{1}{2}\pi, \tag{A 35}$$

$$T'_s = K e^{z_f} \cos\theta, \quad \tfrac{1}{2}\pi \leqslant \theta \leqslant \pi. \tag{A 36}$$

(*b*) On $\theta = \frac{1}{2}\pi$, equations (A 14), (A 16) and (A 17) still apply and

$$G = e^{-2z}\, \partial^2\psi'/\partial\theta^2 \quad \text{for} \quad z \geqslant 0. \tag{A 37}$$

(*c*) On $z = 0$, equations (A 19), (A 21) and (A 22) apply and

$$\left.\begin{aligned} G &= Ma \frac{\partial T'_l}{\partial\theta} \sin\theta + 2\left(\frac{\partial^2\psi'}{\partial z^2} - 2\frac{\partial\psi'}{\partial z}\right), \\ \partial T'_l/\partial z &= Bi\,(T'_l - T'_v), \end{aligned}\right\} \quad 0 \leqslant \theta \leqslant \tfrac{1}{2}\pi. \tag{A 38, A 39}$$

(*d*) On $z = 0$, $\frac{1}{2}\pi \leqslant \theta \leqslant \pi$,

$$\partial T'_s/\partial z = 0. \tag{A 40}$$

(*e*) Equations (A 24) and (A 25) are used. L'Hospital's rule is employed to find F and u' as $\theta \to 0$:

$$F = G/e^{2z} \sin^2\theta = (\partial^2 G/\partial\theta^2)/2\,e^{2z}, \tag{A 41}$$

$$u' = -(\partial\psi'/\partial\theta)/e^{2z} \sin\theta = -(\partial^2\psi'/\partial\theta^2)/e^{2z}. \tag{A 42}$$

The equations in z and the velocity components u' and v' at interior nodal points are converted to difference equations using conventional central difference techniques for uniform intervals in z and θ. (Smaller intervals in θ are used near the axes $\theta = 0$ and $\frac{1}{2}\pi$.) The boundary conditions are represented either by one-sided difference expressions or by introducing grid points beyond the physical boundary. Full details of the formulae used are given in Kao (1970). The integral $\int_0^\theta T'_l \sin\theta\, d\theta$ is evaluated by the trapezoidal rule. Simpson's rule, although more accurate, is inconvenient in this case since the integral can be evaluated only at odd grid points.

The difference equations were solved on an I.C.L. KDF 9 computer using the Gauss–Seidal iteration method with over- or under-relaxation. The appropriate value of the relaxation factor was determined by trial and error, and varied between 1·9 at low Ma to as low as 0·5 to achieve stability of the solution at large Ma, low Bi. The calculations were started by using guessed values of T'_l, T'_s ψ' and G to calculate improved values of T'_l and T'_s. The new T'_l was then used to calculate an improved G and thence ψ', u' and v'. The procedure was then repeated until the variables changed by less than a specified tolerance per iteration, usually taken as 10^{-4} except in a few cases, where a tolerance of 10^{-1} was used for G. The choice of initial values not only affected the computation time but also could induce divergence of the solution in some cases. This difficulty was reduced by using the final solution of a calculation at low Ma, high Bi as the initial guess for the next calculation at higher Ma or lower Bi.

REFERENCES

BROWN, W. T. 1967 Ph.D. thesis, Dept. Mechanical Engineering, M.I.T.

GADDIS, E. S. 1968 Ph.D. thesis, Dept. Mechanical Engineering, University of Manchester.

GADDIS, E. S. & HALL, W. B. 1968 *Thermodynamics and Fluid Mechanics Convention, I.Mech. E. Proc.*, **182** (3H), 152.

JENSON, V. G. 1959 *Proc. Roy. Soc.* A **249**, 346.

KAO, Y. S. 1970 D.Phil. thesis, Dept. Engineering Science, Oxford University.

KENNING, D. B. R. 1968 *Thermodynamics and Fluid Mechanics Convention, I. Mech. E. Proc.* **182** (3H), 320.

LARKIN, B. K. 1970 *A.I.Ch.E. J.* **16**, 101.

MCGREW, J. L. BAMFORD, F. L. & REHM, T. R. 1966 *Science*, **153**, 1106.

SCHRAGE, R. W. 1953 *A Theoretical Study of Interphase Mass Transfer*. Columbia University Press.

WILCOX, S. J. & ROHSENOW, W. M. 1969 *Engineering Projects Laboratory, M.I.T. Rep.* DSR 71475-62.